

ARMY RESEARCH LABORATORY



**Self-Assembled, Ultra-Hydrophobic
Micro/Nano-Textured Surfaces**

by Adam M. Rawlett, Joshua A. Orlicki, Afia Karikari, and Tim Long

ARL-TR-3547

August 2005

NOTICES

Disclaimers

The findings in this report are not to be construed as an official Department of the Army position unless so designated by other authorized documents.

Citation of manufacturer's or trade names does not constitute an official endorsement or approval of the use thereof.

Destroy this report when it is no longer needed. Do not return it to the originator.

Army Research Laboratory

Aberdeen Proving Ground, MD 21005-5069

ARL-TR-3547

August 2005

Self-Assembled, Ultra-Hydrophobic Micro/Nano-Textured Surfaces

**Adam M. Rawlett and Joshua A. Orlicki,
Weapons and Materials Research Directorate, ARL**

**Afia Karikari and Tim Long
Virginia Tech University**

REPORT DOCUMENTATION PAGE			Form Approved OMB No. 0704-0188	
Public reporting burden for this collection of information is estimated to average 1 hour per response, including the time for reviewing instructions, searching existing data sources, gathering and maintaining the data needed, and completing and reviewing the collection information. Send comments regarding this burden estimate or any other aspect of this collection of information, including suggestions for reducing the burden, to Department of Defense, Washington Headquarters Services, Directorate for Information Operations and Reports (0704-0188), 1215 Jefferson Davis Highway, Suite 1204, Arlington, VA 22202-4302. Respondents should be aware that notwithstanding any other provision of law, no person shall be subject to any penalty for failing to comply with a collection of information if it does not display a currently valid OMB control number. PLEASE DO NOT RETURN YOUR FORM TO THE ABOVE ADDRESS.				
1. REPORT DATE (DD-MM-YYYY) August 2005		2. REPORT TYPE Final		3. DATES COVERED (From - To) June 2004–September 2004
4. TITLE AND SUBTITLE Self-Assembled, Ultra-Hydrophobic Micro/Nano-Textured Surfaces			5a. CONTRACT NUMBER	
			5b. GRANT NUMBER	
			5c. PROGRAM ELEMENT NUMBER	
6. AUTHOR(S) Adam M. Rawlett, Joshua A. Orlicki, Afia Karikari, * and Tim Long *			5d. PROJECT NUMBER AH84	
			5e. TASK NUMBER	
			5f. WORK UNIT NUMBER	
7. PERFORMING ORGANIZATION NAME(S) AND ADDRESS(ES) U.S. Army Research Laboratory ATTN: AMSRD-ARL-WM-MA Aberdeen Proving Ground, MD 21005-5069			8. PERFORMING ORGANIZATION REPORT NUMBER ARL-TR-3547	
9. SPONSORING/MONITORING AGENCY NAME(S) AND ADDRESS(ES)			10. SPONSOR/MONITOR'S ACRONYM(S)	
			11. SPONSOR/MONITOR'S REPORT NUMBER(S)	
12. DISTRIBUTION/AVAILABILITY STATEMENT Approved for public release; distribution is unlimited.				
13. SUPPLEMENTARY NOTES *Department of Chemistry, Virginia Tech University, Blacksburg, VA				
<p>Hierarchical self assembly of nano-scale components (i.e., abalone shells, etc.) has been perfected by nature, yet the ability for scientists to utilize similar techniques is still in its infancy. The assembly of complex nano- and micro-components via self organizing means, rather than serial or parallel processing methods (e.g., electron beam lithography or nano-imprinting, respectively), could exploit the inherent benefit of these entities in a more elegant, economic means.</p> <p>The self assembly of regular arrays of nano- and microscale pores in polymer matrices, generated by so-called breath figures, will be discussed. Experimental parameters to vary the size, spacing, organization, long-range order, etc., of these self-organizing surfaces will also be discussed. Utilizing these regular arrays of pores as templates, we have patterned analogous arrays of pillars (inverse pores) from a polymer film cast onto the patterned surface. These micro-/nano-textured surfaces have greatly enhanced the hydrophobicity of the textured polymer when measured by contact angle. This method of producing ultra-hydrophobic textured surfaces should be amenable to high-throughput, low-cost manufacturing of myriad polymeric surfaces.</p>				
15. SUBJECT TERMS breath figures, self assembly, hydrophobic				
16. SECURITY CLASSIFICATION OF:			17. LIMITATION OF ABSTRACT UL	18. NUMBER OF PAGES 18
a. REPORT UNCLASSIFIED	b. ABSTRACT UNCLASSIFIED	c. THIS PAGE UNCLASSIFIED		
				19b. TELEPHONE NUMBER (Include area code) 410-306-0695

Contents

List of Figures	iv
List of Tables	iv
1. Background	1
2. Experimental Procedure	2
2.1 Materials and Instrumentation.....	2
2.2 Breath Figure Formation	2
2.3 Silicon Rubber Pillar Formation.....	3
3. Results and Discussion	3
3.1 Effect of Molecular Weight on Breath Figure Formation.....	3
3.2 Effect of Concentration on Breath Figure Formation	6
3.3 Effect of Humidity Level on Breath Figure Formation.....	6
4. Templating From Breath Figures	7
5. Conclusions	10
6. References	11
Distribution List	12

List of Figures

Figure 1. Schematic of breath figure formation (5).....	2
Figure 2. Optical micrographs of variable molecular weight PS breath figures formed in CH_2Cl_2 (7 weight-percent) at 72% RH from left to right: 20-, 51-, and 160-kDa polystyrene.....	4
Figure 3. A series of confocal laser micrographs of PS 51-kDa breath figures formed in CH_2Cl_2 (7 weight-percent) at 73% RH. (A) Low magnification ($10\times$, $921 \times 921 \mu\text{m}$ at a wavelength of 458 nm), (B) medium magnification ($20\times$, $461 \times 461 \mu\text{m}$ at a wavelength of 633 nm), (C) high magnification ($50\times$, $184 \times 184 \mu\text{m}$ at a wavelength of 458 nm).....	4
Figure 4. AFM images of different molecular weight PS breath figures formed in CH_2Cl_2 (7 weight-percent) at 72% RH.....	5
Figure 5. AFM images of PS (160-kDa) breath figures formed in CH_2Cl_2 at different concentrations and 72% RH.....	6
Figure 6. Optical micrographs of PS breath figures (7 weight-percent) formed in CH_2Cl_2 at different humidity levels: (a) and (b) are 20- and 51-kDa PS formed at 68% RH, respectively, while c and d are 20 and 51 kDa formed at 72% RH, respectively.....	7
Figure 7. Three-dimensional AFM images of silicon rubber pillars formed on breath figure template. In (a), the silicon rubber was crosslinked on a 51-kDa PS breath figure film formed in an uncontrolled environment, while for (b), it was crosslinked on a PS film of the same molecular formed in a humidity chamber at 73% RH.....	8
Figure 8. AFM and optical images of silicon pillars (GE Silicons RTV 615 silicon rubber) - (a) 3-D AFM image of the breath figure template before coating, (b) optical micrograph of the pillars, (c) 3-D AFM image of the pillars.....	8
Figure 9. AFM images of silicon rubber pillars (Dow Corning 3120 RTV silicon rubber) - (a) the breath figure template before coating, (b) optical micrograph of the pillars, (c) atomic force micrograph of the pillars.....	8
Figure 10. Typical defects observed in silicon pillar formation: (a) optical micrograph of a cluster of pillars, (b) the corresponding AFM image and (c) AFM image obtained after pillars were improperly peeled.....	9
Figure 11. Contact angle measurement (goniometer) - left: cured Si rubber (control) advancing CA = 100° , receding = 90° , right: cured Si rubber with pillars CA = 135° , receding = 127°	9

List of Tables

Table 1. Average diameter and depth of PS pores as a function of molecular weight at 72% RH measured via AFM.....	5
Table 2. Average diameter and depth of PS pores as a function of concentration at 72% RH measured by AFM.....	6

1. Background

The formation of hierarchically ordered arrays of spherical cavities on polymer films is of interest due to potential applications in the preparation of photonic bandgap materials, environmental sensors, and patterned light-emitting diodes (LED). While many methods are known for the preparation of these porous materials, the breath figure approach has received significant scrutiny because of the simple and robust mechanism of pattern formation (1, 2). Breath figures are patterned arrays of micrometer-sized defects in a polymer film, formed when water droplets condensed onto a polymer solution surface during film drying. By controlling variables such as relative humidity and solvent, the feature size and uniformity of the resultant pattern can be controlled. The breath figure approach is valuable because it provides the advantages of large area ordering in the nano and micrometer regime, is versatile, and inexpensive.

The process is driven by the evaporation of an appropriate solvent under humid conditions, leading to a decrease in temperature at the air-liquid interface, resulting in water condensation (3). The drop-wise condensation proceeds according to several steps shown in figure 1. The first stage involves nucleation of the water droplets on the polymer-solution surface. During the second stage, the droplets become large enough to touch and coalesce as a result of the self-similarity of the pattern and an acceleration of growth. With properly controlled conditions, a subsequent ordering of the droplets into a hexagonal lattice is observed (4). The temperature difference between the surface and the ambient conditions is minimized once the surface of the film is covered with water droplets. At this stage, the water droplets may sink into the solution (depending upon solution density). Upon complete evaporation of the solvent, the pattern of the droplets generated in the polymer matrix is preserved as a hexagonally ordered array of pores with a honeycomb structure (5, 6).

The self assembly of regular arrays of nano and microscale pores in polymer matrices generated using the breath figure technique will be discussed. Experimental parameters to vary the size, spacing, organization, and long range order of these self-organizing surfaces will also be discussed. Utilizing these regular arrays of pores as templates we have patterned analogous arrays of pillars (inverse pores) from a polymer film cast onto the patterned surface. These micro/nano-textured surfaces have enhanced the hydrophobicity of the textured polymer when measured by contact angle. This method of producing ultra-hydrophobic textured surfaces should be amenable to high-throughput, low-cost manufacturing of myriad polymeric surfaces.

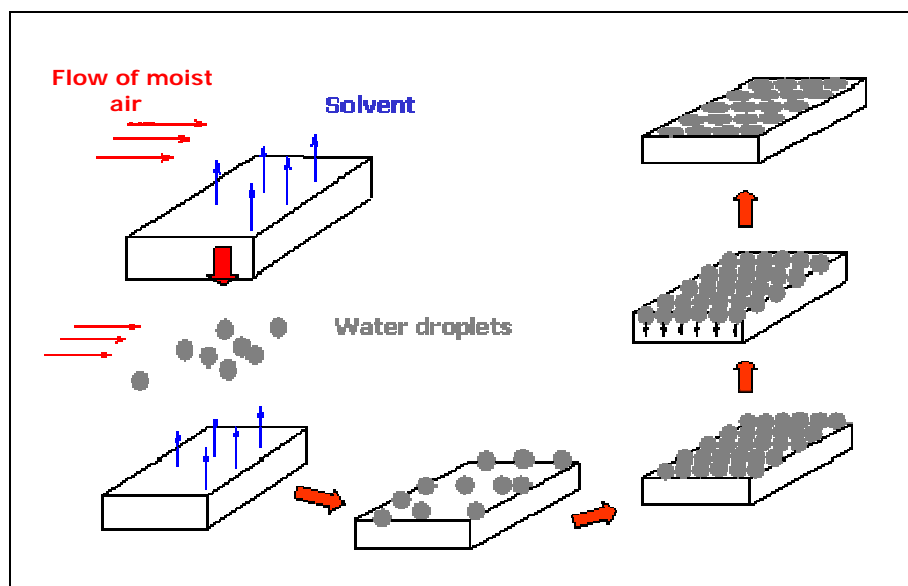


Figure 1. Schematic of breath figure formation (5).

2. Experimental Procedure

2.1 Materials and Instrumentation

Polystyrene with a series of molecular weights ($M_n = 10, 19.8, 51, 160, \text{ and } 411 \text{ kDa}$, polydispersity index (PDI) = 1.06 for all the polymers) were purchased from Pressure Chemical Company. These materials were used to form the breath figure pores.

In order to prepare the array of pillars, two different silicon rubbers were evaluated. A high-viscosity, opaque rubber was obtained from Dow Corning 3120 RTV Silicon Rubber; GE Silicons provided a clear, low-viscosity resin, RTV615.

Atomic force microscopy (AFM) images were obtained on a Dimension 3100 AFM equipped with a Nanoscope* IV scanning probe microscope controller. Laser scanning confocal micrographs were taken with a Zeiss Pascal 5 confocal microscope equipped with two helium lasers and a multiwavelength Argon laser. Scanning electron microscopy (SEM) was performed using a Hitachi S-4700 instrument equipped with a field-emission cathode.

2.2 Breath Figure Formation

A humidity chamber was created using a plastic desiccator with a nitrogen inlet and outlet. To impose a relative humidity of 65–80%, a saturated sodium chloride salt solution covered with

*Nanoscope is a trademark of Veeco Instruments, Inc., Woodbury, NY.

Parafilm* wrap was placed in the chamber at ambient temperature. A 20-mL disposable syringe barrel was inverted and used to bubble nitrogen gas through the saturated salt solution at a controlled rate. The relative humidity was measured with a digital Dickson hygrometer and could be controlled by changing the gas velocity. The polymer solutions (1.0–10.0 weight-percent) were prepared by weighing the required amount of polystyrene (PS) into a sample vial and dissolving it in dry methylene chloride (CH_2Cl_2). The substrate, a Kapton[†] polyimide film (thickness of 127 μm) was cut to the required size, rinsed twice with ethanol, and dried with nitrogen. The film was ozone treated for 20 s, taped to a standard glass microscope slide and then placed in the humidity chamber. A 1.0-mL drop of the polystyrene solution was placed on the substrate in the humidity-controlled chamber, and the solvent was allowed to evaporate at room temperature at the required relative humidity.

2.3 Silicon Rubber Pillar Formation

In order to prepare the array of pillars two different silicon rubbers were evaluated. Both systems required the mixing of a 10:1 mixture of silicon rubber prepolymer and catalyst. After thorough mixing, the resin was degassed under vacuum for 20 min. After mixing, the silicon resin was then coated via pipette on the PS breath figures. The samples were subsequently cured in an oven at 60 °C for 16 hr. Selected samples were post-cured at 120–130 °C for 4 hr. After curing, the samples were cooled to room temperature and then cut into two equal portions. One sample was developed (removed from the PS-breath figure substrate) by dissolution, the other by mechanical separation. For the dissolution route, tetrahydrofuran (THF) was used to selectively dissolve the PS breath figure leaving behind an array of pillars. The mechanical separation entailed the peeling-apart of the PS and silicon rubber films. While the mechanical method was faster, some level of surface damage was observed due to strong physisorption.

3. Results and Discussion

3.1 Effect of Molecular Weight on Breath Figure Formation

A 7 weight-percent PS solution was prepared for four different molecular weights: 10, 19.8, 51, and 160 kDa in CH_2Cl_2 . A 1.0-mL drop of each solution was deposited on ozone-treated Kapton films in a humidity chamber at 72% relative humidity (RH) with constant nitrogen flow. The surface of the polymer solutions became turbid, indicating breath figure formation. Figure 2 shows the optical micrographs of the breath figures generated from various molecular weight PS solutions under the same conditions. The morphologies of the five films were significantly different, confirming molecular weight as a key parameter influencing pattern formation.

*Parafilm is a registered trademark of American Can Company, Greenwich, CT.

[†] Kapton is a registered trademark of Dupont, Circleville, OH.

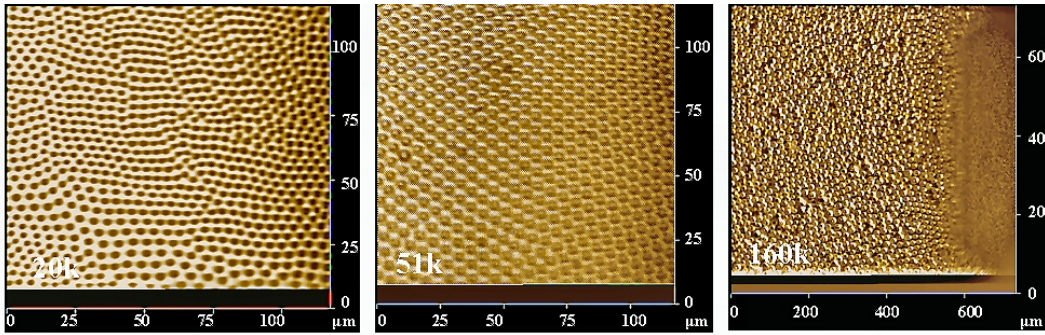


Figure 2. Optical micrographs of variable molecular weight PS breath figures formed in CH_2Cl_2 (7 weight-percent) at 72% RH from left to right: 20-, 51-, and 160-kDa polystyrene.

For the 10-kDa film, the edges of the film scattered light (i.e., appeared turbid) while the central area remained clear. The optical micrograph for this film (not shown) established the presence of a few pores on the outskirts of the film and not on the remaining parts. In the case of the 20-kDa PS film, pores were observed uniformly across the surface but the order was confined to several small domains. Highly ordered pores were obtained for PS with a molecular weight of 51 kDa, as can be seen in figure 2 (center image). The pores in the 160-kDa film were disordered. Examination of the 51-kDa film using laser scanning confocal microscopy (figure 3) also confirmed the hexagonally packed highly ordered honeycomb structures of the 51-kDa PS.

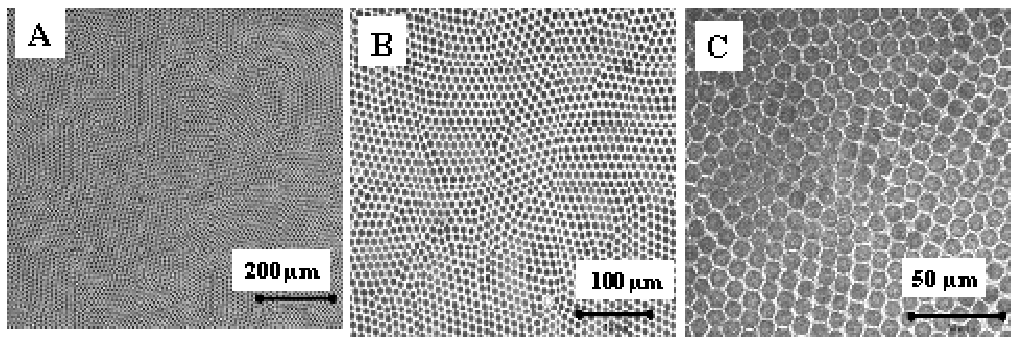


Figure 3. A series of confocal laser micrographs of PS 51-kDa breath figures formed in CH_2Cl_2 (7 weight-percent) at 73% RH. (A) Low magnification (10 \times , 921 \times 921 μm at a wavelength of 458 nm), (B) medium magnification (20 \times , 461 \times 461 μm at a wavelength of 633 nm), (C) high magnification (50 \times , 184 \times 184 μm at a wavelength of 458 nm).

AFM images confirmed the optical microscope observations as shown in figure 4. The number-average diameter (D_n) and depth of the pores for the various molecular weights were determined by AFM and are summarized in table 1. Please note that depth and diameter measurements of the formed pores may be affected by the AFM tip geometry and will be further verified by confocal microscopy.

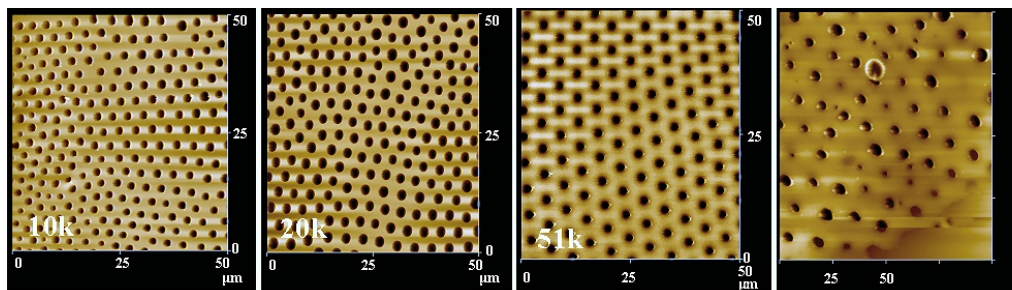


Figure 4. AFM images of different molecular weight PS breath figures formed in CH_2Cl_2 (7 weight-percent) at 72% RH.

Table 1. Average diameter and depth of PS pores as a function of molecular weight at 72% RH measured via AFM.

Molecular Weight (g/mol)	Diameter (μm)	Depth (μm)	Interval (μm)
10	2.3 ± 0.3	1.3 ± 0.2	1.2 ± 0.1
20	2.5 ± 0.2	2.2 ± 0.2	1.3 ± 0.1
51	3.4 ± 0.7	0.5 ± 0.1	1.6 ± 0.4
160	4.9 ± 1.2	1.2 ± 0.2	8.4 ± 1.4

As can be seen in table 1, there was no direct correlation observed between molecular weight and pore depth. The average values ranged from 1.2 to $2.2 \pm 0.2 \mu\text{m}$. It is not known why the highly ordered pores of the 51-kDa PS film had an average depth of 500 nm, although, it could arise from the inability of the AFM tip to fully trace the depth of the pore. Pore diameters, D_n , on the other hand, were found to increase with increasing molecular weight and become more polydisperse. The D_n for the different molecular weights at 72% RH ranged from 2.3 to $4.9 \mu\text{m}$ while the interval between adjacent pores also increased with increasing molecular weight. The same experiment was attempted for a 411-kDa polymer which demonstrated little hierarchical assembly. The results obtained here for 20–160 kDa are consistent with published results for other solvents (6).

The influence of molecular weight upon breath figure formation is related to the viscosity of the polymer in solution. A low molecular weight polymer exhibits a low solution viscosity, permitting the coalescence of water droplets (7) by translational diffusion. This can result in disordered arrays of pores during breath figure formation. On the other hand, a very high molecular weight PS exhibits a high solution viscosity; as such the water droplets are not able to diffuse across the surface, leading to fewer pores in the films (figure 3). The results obtained for the 10-kDa film were different from those expected for a low-molecular-weight sample, as only a few ordered pores were observed. This result can be attributed to the use of CH_2Cl_2 in the film preparation, compared to CHCl_3 and toluene used in other published works (7). The higher vapor pressure of CH_2Cl_2 combined with the low molecular weight allowed for faster evaporation in the 10-kDa PS film. As a consequence, low overall viscosity of the 10-kDa sample resulted in preservation of the breath figure only at the edges, and only in poor fashion.

3.2 Effect of Concentration on Breath Figure Formation

As mentioned, the viscosity of the polymer solution plays an important role in the formation of regular breath figures. In this experiment, a series of PS solutions (160 kDa) ranging from 1.0 to 7.0 weight-percent were prepared and studied at 72% RH (figure 5). Highly ordered pores with monodisperse pore dimensions were observed for the 1.0-weight-percent PS film while the pores became more disorganized with increasing concentration. An increase in concentration was accompanied by an increase in pore size polydispersity, leading to defects in the array formation (observed for the 7-weight-percent film in figure 5).

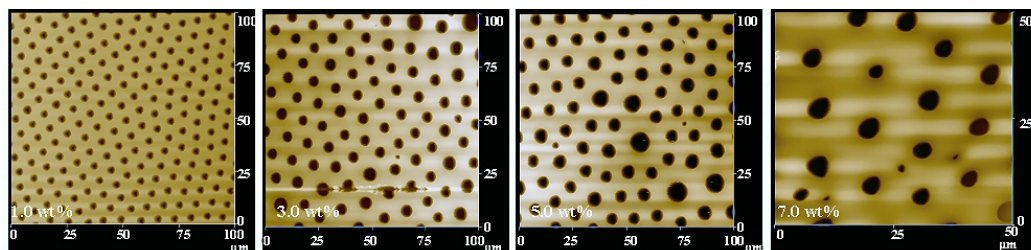


Figure 5. AFM images of PS (160-kDa) breath figures formed in CH_2Cl_2 at different concentrations and 72% RH.

From the summarized results in table 2, it is evident that the pore sizes became larger and more irregular as the concentration increased from 1.0 to 7.0 weight-percent. The average interval between adjacent pores was found to increase from $2.3 \pm 0.4 \mu\text{m}$ to $9.5 \pm 1.0 \mu\text{m}$. A 10-weight-percent PS solution was prepared but the results were inconclusive.

Table 2. Average diameter and depth of PS pores as a function of concentration at 72% RH measured by AFM.

Concentration (Weight-Percent)	Diameter (μm)	Depth (μm)	Interval (μm)
1.0	4.1 ± 0.3	3.1 ± 0.2	2.3 ± 0.4
3.0	6.0 ± 0.6	2.8 ± 0.5	5.0 ± 0.4
5.1	6.6 ± 0.7	4.1 ± 0.6	5.0 ± 0.9
7.0	5.9 ± 1.6	3.7 ± 0.8	9.5 ± 1.0

3.3 Effect of Humidity Level on Breath Figure Formation

In figure 6, the effect of humidity on breath figure formation in CH_2Cl_2 was studied for 20- and 51-kDa PS solutions at 68% and 72% RH. At 68% RH, highly disordered pores with several defects were observed in the 20-kDa PS film (figure 6a). For a 51-kDa solution under the same conditions, smaller pockets of ordered structures were obtained with a reduced number of defects as shown by the optical micrograph in figure 6b. An increase in the humidity level from 68% to 72% produced significant improvement of the morphology of two films as can be seen in figures 6c and figure 6d. Complete suppression of the defects was observed. Increasing the humidity level directly increased the pore sizes. At low humidity levels (<40% RH), no breath figures

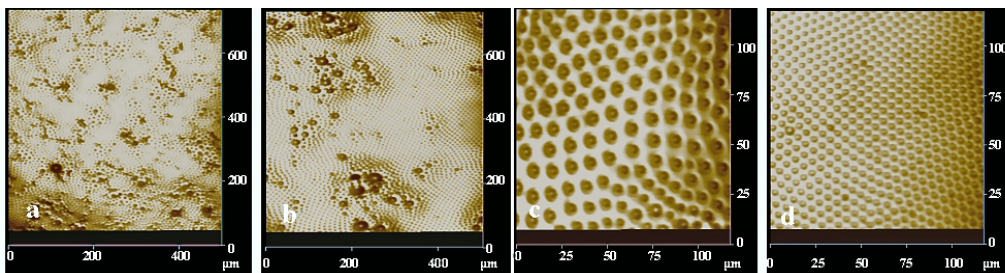


Figure 6. Optical micrographs of PS breath figures (7 weight-percent) formed in CH_2Cl_2 at different humidity levels: (a) and (b) are 20- and 51-kDa PS formed at 68% RH, respectively, while c and d are 20 and 51 kDa formed at 72% RH, respectively.

are observed; at very high humidity levels ($>90\%$), the rapidly condensing water droplets lead to coalescence of the droplets, subsequently resulting in disordered pattern formation and significant increases in the pore dimensions (8, 9). While a strong linear relationship between humidity level and pore sizes is expected, no direct correlations were observed for this system.

4. Templating From Breath Figures

There has been an increase in the amount of research focused on the formation of organized arrays of silicon pillars (10). Tailored surface morphology allows control over wetting characteristics and optical appearance (e.g., matte vs. glossy). As an example, ultra-hydrophobic surfaces were developed from electron-beam defined arrays of micron sized pillars (10). Arrays of softer materials, such as high-aspect ratio polymer fibers, have been implemented in a biomimetic fashion to prepare non sticky adhesives, mimicking the morphology found on a gecko's foot pad (11).

Breath figure arrays such as those described in the last section, will be used as templates in an effort to generate micrometer-sized silicon rubber pillars, which may possess some properties analogous to those described previously. The pillars were obtained by infiltrating the PS breath figures with two types of silicon rubber, crosslinking the rubber and then removing the PS template by peeling the layers apart or by dissolving the PS in THF. Figure 7 depicts pillars formed by coating silicon rubber on disordered (a) and ordered (b) breath-figure templates. The average diameter of the ordered array of pillars (figure 7b) was $4.5 \pm 0.2 \mu\text{m}$, with a height of about $1.0 \mu\text{m}$ (removed by peeling).

In figures 8 and 9, the AFM images of silicon pillars formed by coating the PS pores with a colorless low viscosity rubber (GE Silicons RTV 615) (figure 8c) and a red, highly viscous (figure 9c) silicon rubber (Dow Corning 3120 RTV) are shown with the their corresponding breath-figure templates and optical micrographs (removed by peeling).

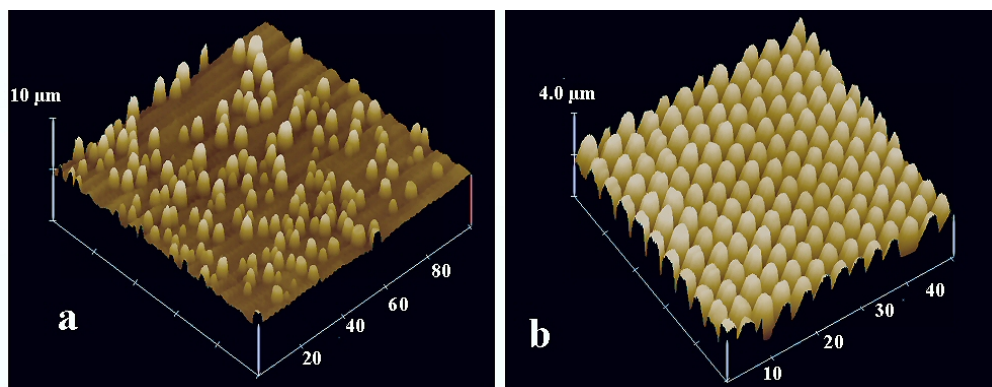


Figure 7. Three-dimensional AFM images of silicon rubber pillars formed on breath figure template. In (a), the silicon rubber was crosslinked on a 51-kDa PS breath figure film formed in an uncontrolled environment, while for (b), it was crosslinked on a PS film of the same molecular formed in a humidity chamber at 73% RH.

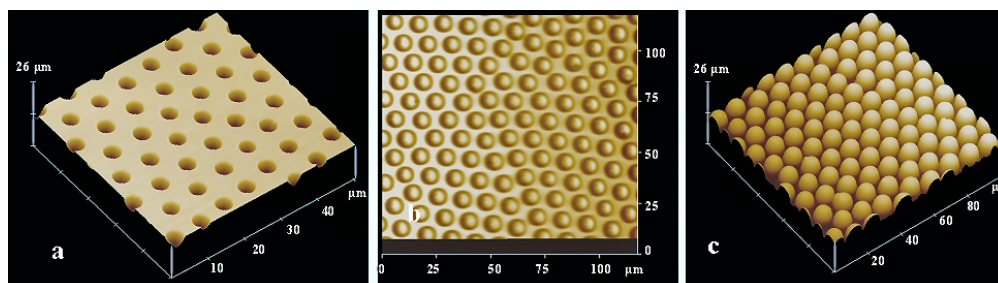


Figure 8. AFM and optical images of silicon pillars (GE Silicons RTV 615 silicon rubber) - (a) 3-D AFM image of the breath figure template before coating, (b) optical micrograph of the pillars, (c) 3-D AFM image of the pillars.

In figure 8a, the average pore diameter and depth were $4.4 \pm 0.1 \mu\text{m}$ and $3.0 \pm 0.3 \mu\text{m}$, respectively. On the other hand, the corresponding pillar diameter and depth (figure 8c) were $10.6 \pm 0.3 \mu\text{m}$ and $3.7 \pm 0.4 \mu\text{m}$, respectively. The increase in the pore dimensions can be attributed to swelling of the crosslinked pillars as a result of residual solvent since they were developed in THF and dried at 40°C for 2 days. Similar results were obtained for the pillars formed with the highly viscous silicon rubber (figure 9). The average pore diameter and depth were $5.7 \pm 0.2 \mu\text{m}$ and $3.5 \pm 0.6 \mu\text{m}$, respectively (figure 9a) while the pillar diameter and height were $6.5 \pm 1.1 \mu\text{m}$ and $3.9 \pm 0.6 \mu\text{m}$, respectively.

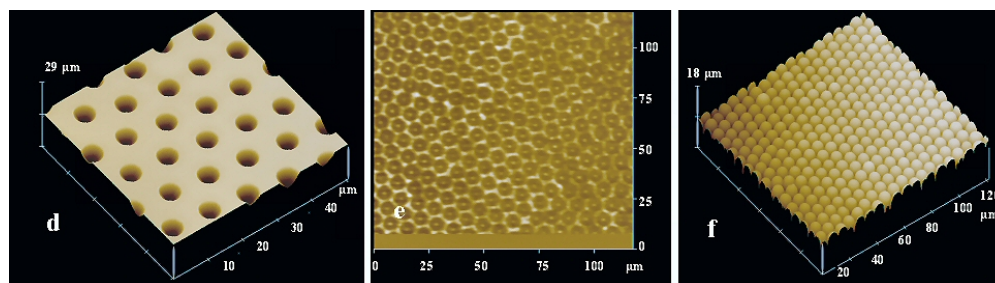


Figure 9. AFM images of silicon rubber pillars (Dow Corning 3120 RTV silicon rubber) - (a) the breath figure template before coating, (b) optical micrograph of the pillars, (c) atomic force micrograph of the pillars.

Figure 10a and 10b show optical and AFM images of typical defects that were observed during the silicon pillar formation. These clusters of pillars were observed when the high-viscosity silicon rubber (Dow Corning 3120 RTV) was crosslinked without proper degassing. Such clusters were not observed with the low viscosity rubber (GE Silicons RTV615). In figure 10c, the AFM image of pillars that were obtained by improperly peeling off the polystyrene template is shown. Red silicon rubber was observed on the PS template after peeling, signifying cohesive failure.

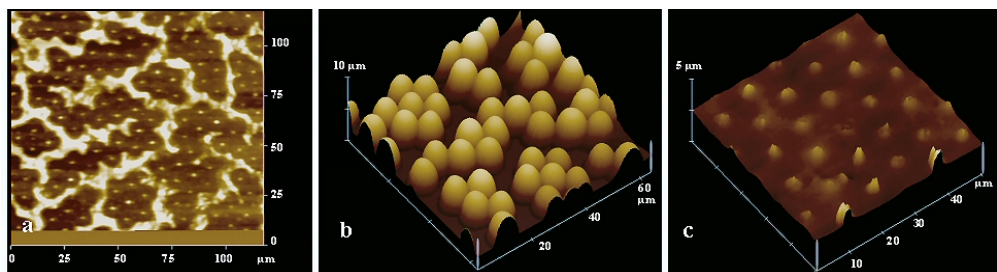


Figure 10. Typical defects observed in silicon pillar formation: (a) optical micrograph of a cluster of pillars, (b) the corresponding AFM image and (c) AFM image obtained after pillars were improperly peeled.

Figure 11 demonstrated the effect of micro patterning through breath-figure templating on polymer surface morphology. Similar to the gecko's foot pad, known for superior dry adhesion, micron roughness greatly enhances surface roughness leading to a large increase in hydrophobicity of a polymer surface. These micro/nano-texturing of the surface have enhanced the hydrophobicity of the polymer when measured by contact angle. This method of producing ultra-hydrophobic textured surfaces should be amenable to high throughput, low-cost manufacturing of myriad polymeric surfaces.

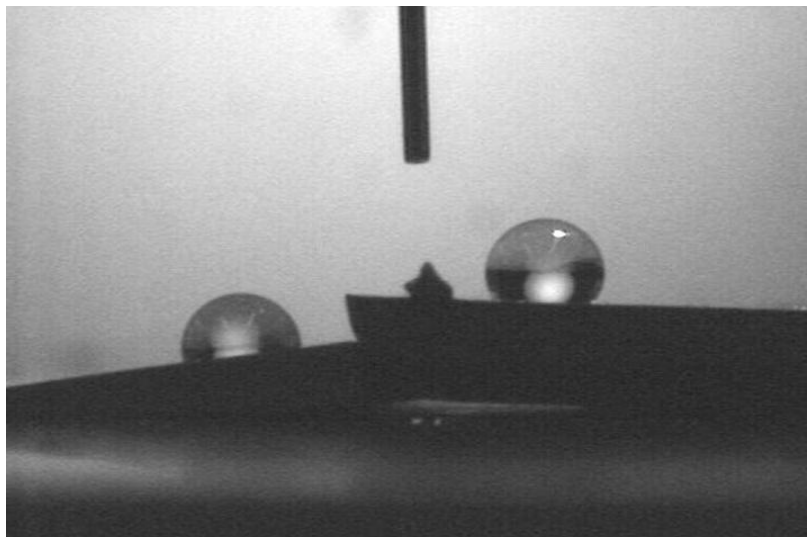


Figure 11. Contact angle measurement (goniometer) - left: cured Si rubber (control) advancing CA = 100° , receding = 90° , right: cured Si rubber with pillars CA = 135° , receding = 127° .

5. Conclusions

In summary, the effect of polymer molecular weight, solution viscosity, concentration, and relative humidity on the formation of ordered arrays of hexagonal pores were examined in CH_2Cl_2 . Molecular weight was shown to strongly influence the formation of the ordered pores. Polystyrene with a low molecular weight (10 kDa) resulted in the formation of only a few pores while a high molecular weight resulted in the formation of disordered and highly polydispersed structures. Also, 7-weight-percent solution concentrations led to the formation of disorganized and polydisperse pore sizes while highly ordered hexagonally packed monodisperse pores with large area ordering was observed for 1.0-weight-percent polystyrene solutions with a molecular weight of 160 kg/mol. A linear correlation was observed between humidity levels and the ordering of the pores. Highly ordered arrays of silicon rubber pillars were also obtained by using the PS breath figures as templates. These micro-textured surfaces greatly enhanced the hydrophobicity of the polymer when measured by contact angle. This method of producing ultra-hydrophobic textured surfaces should be amenable to high-throughput, low-cost manufacturing of myriad polymeric surfaces.

6. References

1. Yabu, H.; Shimomura, M. Simple Fabrication of Micro Lens Arrays. *Langmuir* **2005**, *21* (5), 1709–1711.
2. Englert, B. C.; Scholz, S.; Leech, P. J.; Srinivasarao, M.; Bunz, U. H. F. Templated Ceramic Microstructures by Using the Breath-Figure Method. *Chem. Eur. J.* **2005**, *11* (3), 995–1000.
3. Boker, A.; Lin, Y.; Chiapperini, K.; Horowitz, R.; Mark, T.; Carreeon, T.-X.; Abertz, C.; Skaff, H.; Dinsmore, A.; Emrick, T.; Russell, T. Hierarchical Nanoparticle Assemblies Formed by Decorating Breath Figures. *Nature Mater* **2004**, *3*, 302–306.
4. Marcos-Martin, M.; Beysens, D.; Bouchaud, J. P.; Godreche, C.; Yekutieli, I. Self-Diffusion and Visited Surface in the Droplet Condensation Problem (Breath Figures). *Physica A* **1995**, *214*, 396–412.
5. Park, M. S.; Kim, K. K. Breath Figure Patterns Prepared by Spin Coating in a Dry Environment. *Langmuir* **2004**, *20*, 5347–5352.
6. Mohan, S.; Collings, D.; Phillips, A.; Patel, S. Three-Dimensionally Ordered Array of Air Bubbles in a Polymer Film, *Science* **2001**, *292*, 79–83.
7. Peng, J.; Han, Y.; Yang, Y.; Binyao, L. The Influencing Factors on the Macroporous Formation in Polymer Films by Water Droplet Templating. *Polymer* **2004**, *45*, 447–452.
8. Gray, J. J.; Klein, D. H.; Korgel, B. A.; Bonnecaze, R. T. Microstructure Formation and Kinetics in the Random Sequential Adsorption of Polydisperse Tethered Nanoparticles Modeled as Hard Disks. *Langmuir* **2001**, *17*, 2317.
9. Steyer, A.; Guenoun, P.; Beysens, D.; Knobler, C. M. Two-Dimensional Ordering During Droplet Growth on a Liquid Surface. *Phys. Rev. B.* **1990**, *42*, 1086–1089.
10. Krupenkin, T. N.; Taylor, J. A.; Schneider, T. M.; Yang, S. From Rolling Ball to Complete Wetting: The Dynamic Tuning of Liquids on Nanostructured Surfaces. *Langmuir* **2004**, *20*, 3824–3827.
11. Sitti, M.; Fearing, R. S. Synthetic Gecko Foot-Hair Micro/Nano-Structures as Dry Adhesives. *Journal of Adhesion Science and Technology* **2003**, *17* (8), 1055–1073.

NO. OF
COPIES ORGANIZATION

1 DEFENSE TECHNICAL
(PDF INFORMATION CTR
ONLY) DTIC OCA
8725 JOHN J KINGMAN RD
STE 0944
FORT BELVOIR VA 22060-6218

1 US ARMY RSRCH DEV &
ENGRG CMD
SYSTEMS OF SYSTEMS
INTEGRATION
AMSRD SS T
6000 6TH ST STE 100
FORT BELVOIR VA 22060-5608

1 INST FOR ADVNCD TCHNLGY
THE UNIV OF TEXAS
AT AUSTIN
3925 W BRAKER LN STE 400
AUSTIN TX 78759-5316

1 DIRECTOR
US ARMY RESEARCH LAB
IMNE ALC IMS
2800 POWDER MILL RD
ADELPHI MD 20783-1197

3 DIRECTOR
US ARMY RESEARCH LAB
AMSRD ARL CI OK TL
2800 POWDER MILL RD
ADELPHI MD 20783-1197

3 DIRECTOR
US ARMY RESEARCH LAB
AMSRD ARL CS IS T
2800 POWDER MILL RD
ADELPHI MD 20783-1197

ABERDEEN PROVING GROUND

1 DIR USARL
AMSRD ARL CI OK TP (BLDG 4600)